IJST, Transactions of Mechanical Engineering, Vol. 35, No. M2, pp 121-132
Printed in The Islamic Republic of Iran, 2011

EFFECT OF DENSITY RATIO ON THE HYDRODYNAMIC INTERACTION BETWEEN TWO DROPS IN SIMPLE SHEAR FLOW*

M. BAYAREH[1**] AND S. MORTAZAVI[2]

[1]Dept. of Mechanical Engineering, Lamerd Branch, Islamic Azad University, Lamerd, I. R. of Iran
Email: mbayareh@iaulamerd.ac.ir
[2]Dept. of Mechanical Engineering, Isfahan University of Technology, 84156-8311, Isfahan, I. R. of Iran

Abstract– The effect of density ratio on the hydrodynamic interaction between two drops in simple shear flow at finite Reynolds numbers is studied considering the gravity influence. In this study the full Navier-Stokes equations are solved by a finite difference/front tracking method. The interaction of two drops contains approach, collision, and separation. For a range of density ratios, the interaction between deformable drops increases the cross-flow separation of their centres. The distance between the drop centres along the velocity gradient direction increases irreversibly after collision and reaches a new steady-state value after separation. The interaction between drops is affected by the density ratio. As the density ratio increases, the final equilibrium position of drops moves to the higher velocity region and the drop deformation increases. Drop deformation prevents drop coalescence at finite Reynolds numbers; the reduced collision cross-section of the drops allows them to glide past each other. The drops accelerate while sliding over each other. As the density ratio decreases, drops rotate more slowly, and the point at which the drops separate is delayed.

Keywords– Shear flow, front-tracking method, finite difference method, Reynolds number, Capillary number, Froude number

1. INTRODUCTION

The behavior of rigid and deformable particles in dilute and concentrated suspensions in shear flows has always been of great interest. Dynamics of rigid or deformable drops in a shear flow has been studied for several decades using analytical, numerical and experimental methods. Many of those were restricted to the Stokes and potential flows.

Migration of a single drop in shear flow has been the subject of many investigations. Karnis et al. [1] reported that deformable buoyant particles stabilized midway between the centreline and the wall in a channel. The equilibrium position was closer to the wall for larger flow rates and closer to the centre for larger particles. Similar phenomenon has been observed during migration of a rigid or deformable particle. Two-dimensional simulations of Feng et al. [2] showed that a neutrally buoyant rigid particle migrates to the centerline in a Couette flow and the stagnation pressure on the particle surface is particularly important in determining the direction of migration. Three-dimensional simulations by Doddi and Bagchi [3] on the capsule migration showed that the migration velocity and capsule deformation increase with increasing Capillary number and decrease with increasing viscosity ratio. Bayareh and Mortazavi [4] studied the motion of a single drop in simple shear flow at finite Reynolds numbers. They showed the centreline of the channel is a stable equilibrium position for the drop, and after an initial transient, the drop leads the local ambient fluid velocity.

*Received by the editors November 7, 2010; Accepted September 8, 2011.
**Corresponding author

To simulate the flow of a concentrated suspension successfully, the calculation procedure must be able to describe the interaction of two closely interacting drops. Hydrodynamic interaction between a pair of drops may result in coalescence, breakup or gliding past each other. Magna and Stone [5] reported the time-dependent interactions between two buoyancy-driven deformable drops in a low Reynolds number flow. They introduced three modes for film drainage between the drops: rapid drainage, uniform drainage and dimple formation. As the separation distance between the two drops decreases, the mode of film drainage may change from rapid drainage to uniform drainage and eventually a dimple may form. Zhou and Pozrikidis [6] studied the flow of periodic suspension of two-dimensional viscous drops in a channel bounded by two parallel plane walls. They found that there exists a critical Capillary number below which the suspensions exhibit stable periodic motion, and above which the drops elongate and tend to coalesce, altering the topology of the initial configuration. They studied the effects of Capillary number, viscosity ratio, volume fraction, lattice geometry, and instantaneous drop shape, on the effective stress tensor of the suspension. Li, Zhou and Pozrikidis [7] studied the motion of two-dimensional, doubly periodic, dilute and concentrated emulsions of liquid drops with constant surface tension in a simple shear flow. Loewenberg and Hinch [8] did a three-dimensional simulation of a concentrated emulsion in a shear flow, at zero Reynolds number. Results were obtained for dispersed-phase volume fractions up to 30% and dispersed to continuous-phase viscosity ratios in the range of 0 to 5. They reported that the viscosity of an emulsion is only a weakly increasing function of the dispersed-phase volume fraction.

The collision of two equal-sized drops immersed in an immiscible liquid phase undergoing a shear flow in a parallel apparatus was investigated by Guido and Simeone [9] over a range of Capillary numbers. Trajectories of a pair of drops and their deformations were presented. Experimental investigations on the process of satellite droplet formation by unstable binary collisions were made by Brenn [10]. They presented a theoretical model for the breakup of cylindrical liquid filaments in head-on collision and off-center collision. Also, experimental investigations and numerical simulations of binary droplet collisions using Newtonian and non-Newtonian fluids were performed by Motzigemba et al. [11]. They showed that at all stages of the collision process there are areas in which the velocity gradients for the shear flow are larger than the elongated ones, and vice versa. Balabel et al. [12] introduced a numerical model based on the level set method for computing unsteady droplet internal flows. They presented this model for linear droplet oscillation processes. The simulations by Pan and Suga [13] cover four major regimes of binary collision: bouncing, coalescence, reflexive separation, and stretching separation. Yoon et al. [14] investigated the effect of viscosity ratio on the flow-induced coalescence of two equal-sized drops with clean interfaces experimentally. Effects of inertia on the rheology of a dilute emulsion of drops in shear flow were investigated by Zhao [15] using direct numerical simulation. The drop shape and flow were computed by solving the Navier-Stokes equations in two phases using front tracking method. The collision outcomes of immiscible drops with large surface tension, namely a water drop and a diesel oil drop, were observed experimentally by Chen et al. [16]. They reported no coalescence could be observed for a collision at Weber numbers greater than 60. The deformation of a drop suspended in a shear flow was measured by Sibillo et al. [17] and Zhao [18]. Zhao showed that the final drop size distribution intimately links to the drop break up mechanism, which depends on viscosity ratio and Capillary number.

Lac and Biesel (2008) [19] used a boundary integral formulation to investigate the collision of two identical capsules in simple shear flow. Each capsule consisted of a viscous liquid drop enclosed by an elastic membrane. The hydrodynamic interaction was characterized by an irreversible cross-flow displacement after the capsules had crossed each other. They showed that for sufficiently spaced trajectories, the capsules exhibit negative deflections which displace them to closer streamlines. Gu et al. [20] employed a novel two-phase lattice Boltzmann method (LBM) to study droplet impact dynamics in the presence of surrounding lighter phase. Zhongguo et al. [21] simulated the binary collision of two identical liquid drops using moving particle semi-implicit method. They investigated head-on collision

and eccentric impact. They obtained mass transfer properties by tracking the movement of particles. Nikolopoulos et al. [22] employed the finite volume ethodology coupled with the Volume of Fluid (VOF) technique to simulate the non-central binary collision of two equal size drops in a gaseous phase. Bayareh and Mortazavi [23, 24] simulated the interaction between two equal-size drops using a finite difference/front tracking method. They studied the effects of geometry, viscosity ratio, and drop sizes on the collision of drops neglecting the gravity influence. They observed that the interaction between deformable drops increases the cross-flow separation of their centres. As the viscosity ratio increases, the drops rotate more slowly, and the point at which the drops separate is delayed. Nikolopoulos and Bergeles [25] investigated the effects of liquid and gas properties and droplet size ratio on the collision between two unequal-size drops for the reflexive regime. They reported that the Reynolds number based on the gas properties is not an important parameter affecting the collision of drops.

In this work, the effect of density ratio on the hydrodynamic interaction between two drops in simple shear flow at finite Reynolds numbers is presented. Also, the gravity influence is considered.

The paper is organized as follows: the formulation, introduction of the governing non-dimensional parameters and a short description of the numerical method are discussed in section 2. The results are reported in section 3. The effect of density ratio is also addressed in this section. Section 4 contains the concluding remarks.

2. FORMULATION AND NUMERICAL METHOD

a) Formulation

The governing equations for the motion of unsteady, viscous, incompressible, immiscible two- fluid systems are the Navier-Stokes equations in conservative form:

$$\frac{\partial \rho \mathbf{u}}{\partial t} + \nabla . \rho \mathbf{u}\mathbf{u} = -\nabla P + \nabla . \mu (\nabla \mathbf{u} + \nabla \mathbf{u}^T) + \sigma \int \kappa \mathbf{n} \delta^{\beta} (\mathbf{x} - \mathbf{X}) ds + \rho \mathbf{g} \qquad (1)$$

Here $\boldsymbol{u}$ is the fluid velocity, p is the pressure, ρ is the fluid density, μ is the fluid viscosity, and σ is the surface tension coefficient. Also, δ^{β} is a two- or three-dimensional delta function, for $\beta = 2$, or $\beta = 3$ respectively. κ is the curvature for two-dimensional flows and twice the mean curvature for three-dimensional flows. $\boldsymbol{n}$ is a unit vector normal to the drop surface pointing outside of the drop. $\boldsymbol{x}$ is the position in Eulerian coordinate and $\boldsymbol{X}$ is the position of front in Lagrangian coordinate and $\boldsymbol{g}$ is the acceleration due to gravity.

Mass conservation is given by

$$\frac{\partial \rho}{\partial t} + \nabla . \rho \mathbf{u} = 0 \qquad (2)$$

Both immiscible fluids are taken to be incompressible, so that the density of a fluid particle remains constant:

$$\frac{D \rho}{Dt} = 0 \qquad (3)$$

This reduces the mass conservation equation to

$$\nabla . \mathbf{u} = 0 \qquad (4)$$

Also, the viscosity of each fluid is constant:

$$\frac{D\,\mu}{Dt} = 0 \tag{5}$$

b) Numerical method

Various numerical methods have been used and developed to simulate two-phase flows. In front capturing methods, the front is directly captured on a regular stationary grid. Examples of the methods include marker-and-cell (MAC), the volume-of-fluid (VOF) and level-set method. In the boundary fitted techniques, a separate grid is used for each phase and appropriate boundary conditions are imposed at the boundaries of the grids. Lagrangian methods where the grid follows the fluid were also used to simulate multi-phase flows. In front tracking methods a moving grid is used to represent the interface and a fixed grid is used for the fluid within each phase. In addition to front tracking methods that are applicable to the full Navier Stokes equations, specialized boundary integral methods are used for both potential and Stokes flows. The front-tracking method is a combination of fixed and moving mesh method. Although an interface grid tracks the interface, the flow is solved on a fixed grid. The interface conditions are satisfied by smoothing the interface discontinuities and interpolating interface forces from the interface grid to the fixed grid.

The equations presented in the last section are solved by a projection method. To compute the momentum advection, the pressure term, and the viscous forces, we use a fixed, regular, staggered MAC grid and discretize the momentum equations using a conservative, second-order centered difference scheme for the spatial variables. An explicit second predictor corrector scheme is used to integrate in time.

For the viscous terms we use standard second-order centered differences with simple averaging of the viscosity at points where it is not defined.

A modified version of the code developed by Unverdi and Tryggvason [26] was used in the computations of this paper.

The Navier-Stokes equations are solved on a fixed grid, but the surface tension is found on the front. Therefore, it is necessary to transfer a quantity that exists at the front to a grid. The interface conditions are satisfied by smoothing the interface discontinuities and interpolating interface forces from the interface grid to the fixed grid.

The force due to surface tension on each element of front is [26]:

$$\delta\mathbf{F}_\sigma = \int_{\Delta S} \sigma\kappa\mathbf{n}\,ds \tag{6}$$

The average surface curvature can be written as [26]:

$$\kappa\mathbf{n} = (\mathbf{n}\times\nabla)\times\mathbf{n} \tag{7}$$

Then, the force on each element surface is [26]:

$$\delta\mathbf{F}_\sigma = \sigma\int_{\sigma A}\kappa\mathbf{n}\,dA = \sigma\int_{\sigma A}(\mathbf{n}\times\nabla)\times\mathbf{n}\,dA = \sigma\oint_S \mathbf{t}\times\mathbf{n}\,ds \tag{8}$$

Here the Stokes theorem has been used to convert the area integral into a line integral along the edges of the element. The integration is over the boundary of each element representing the front. ***t*** and ***n*** are the tangent and the normal vector to each element, respectively. The cross product is a vector that lies on the surface and is normal to the edge of the element. If the element is flat, the net force is zero but if the element is curved, the net force is normal to it when the surface tension is constant.

For any incompressible flow it is necessary to solve an elliptic equation. For the velocity-pressure formulation this is a Poisson equation for the pressure.

Numerical simulations of the collision of two drops in simple shear flow were performed over a range of the governing non-dimensional parameters of the flow. These parameters are: (i) The viscosity ratio $\lambda = \mu_d / \mu_\circ$, where $\mu_\circ$ and μ_d are the viscosities of ambient fluid and of the drop, (ii) The density ratio $\eta = \rho_d / \rho_\circ$, where $\rho_\circ$ and ρ_d are the densities of ambient fluid and of the drop, (iii) The Froude number $Fr = g / H\dot{\gamma}^2$, where H is the height of the channel and $\dot{\gamma} = (u_t - u_b) / H$ is the shear rate. Also, u_t and u_b are top and bottom wall velocities, respectively. (iv) The Reynolds number (particle and bulk Reynolds numbers): $Re_P = \rho_\circ \dot{\gamma} R^2 / \mu_\circ$ and $Re_b = \rho_\circ \dot{\gamma} H^2 / \mu_\circ$, where R is the undeformed drop radius. (v) The Capillary number $Ca = \mu_\circ \dot{\gamma} R / \sigma$, where σ is the interfacial tension. The Capillary number is the ratio of viscous force to surface-tension force, (vi) The Weber number $We = \rho_\circ \dot{\gamma}^2 R^3 / \sigma$. The Weber number is the ratio of inertia force to surface-tension force. It should be pointed out that the Weber number and the Capillary number are related by $We = (Re_b)(Ca)(1/\dot{\gamma})(R/H)^2$, so only one of them should be considered as an independent parameter. Bayareh and Mortazavi [22] showed that the proper non-dimensional number for the interfacial tension at finite Reynolds numbers is the Capillary number. We note that in case where the density ratio differs from one, buoyancy force is present in the flow. The simulation is different from if the experiment is done in space. So, in the present study we include the effect of buoyancy.

It is usual to define a scalar measure of the drop deformation D, (the Taylor deformation) by:

$$D = \frac{L - B}{L + B} \tag{9}$$

where L, B are the major and minor semi-axes of the drop (defined by the largest and smallest distances of the surface from the centre).

In addition, the collision or film drainage time is the time between the points where the centre-to-centre distance is equal to one undeformed drop diameter to the instant of coalescence.

3. RESULTS AND DISCUSSION

The reference system is shown in Fig. 1. The x-axis is parallel to flow direction, the y-axis is parallel to the vorticity direction, and the z-axis is parallel to the velocity gradient. The relative trajectory of the drops is expressed in terms of the differences Δx and Δz, which are distances between the drop centres along the x-axis and the z-axis, respectively.

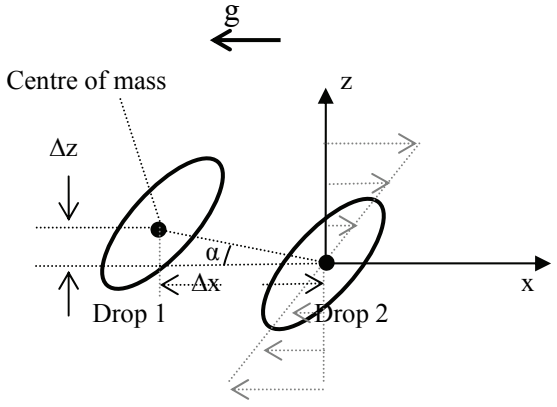

Fig. 1. Collision of two drops in a simple shear flow (Offset = Δz / R)

In all the plots, Δx and Δz will be made dimensionless by radius of the undeformed drops (R). In the simulations presented in this paper, $\lambda = 1$, $Re_b = 10$, $Fr = 392$, and $Ca = 0.3$. We will compare our results

qualitatively with the experimental results of Guido and Simeone [9] ($\lambda = 1$ and $Ca = 0.13$) and Yoon et al. [14] ($\lambda = 1.2$ and $Ca = 0.00417$) and the numerical results of Loewenberg and Hinch [8] ($\lambda = 1$ and $Ca = 0.3$). The conditions chosen are the same as these used by Loewenberg and Hinch [8], but the Capillary number is different from that examined by Guido and Simeone [9].

Since the computational time is directly proportional to the size of the stationary grid, we must find a compromise between the numbers of grid points required to resolve a drop. Figure 2 shows the relative trajectories of two interacting drops computed on $66\times 34\times 66$ and $34\times 18\times 34$ grids. Time is normalized by the shear rate $\dot{\gamma}$. Calculations show slight changes between the two cases. Since the run time depends directly on the size of the grid, we select the coarse grid for our simulations.

Figure 3 shows the sequences (1-5) of the interactions between two drops in simple shear flow at $\eta = 0.1$ on $34\times 18\times 34$ grids. In Fig. 4, Δz is plotted as a function of dimensionless time during approach, collision and separation between the two drops. It can be seen that Δz starts increasing after drops come into apparent contact, reaches a maximum, and, after separation, obtains a new steady-state value. Guido and Simeone [9] experimentally showed that Δz starts increasing where $\Delta x \approx -2R$.

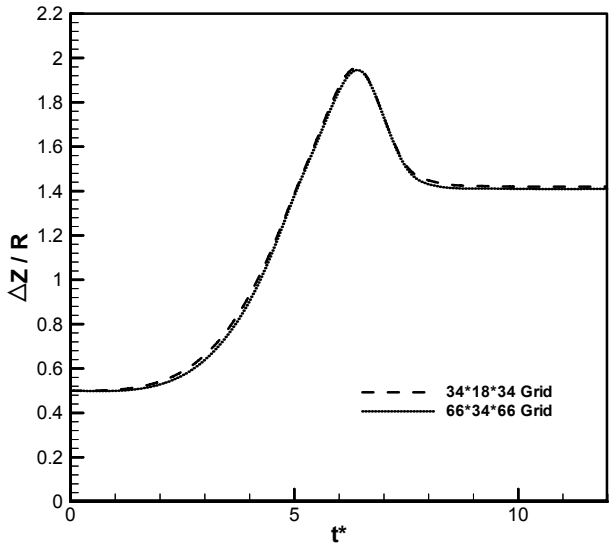

Fig. 2. Relative trajectory of two interacting drops for Ca = 0.05, λ = 1

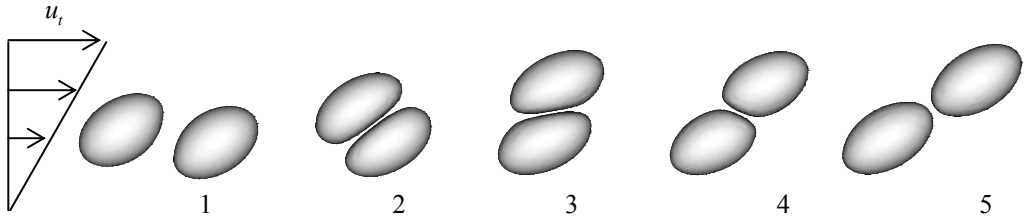

Fig. 3. Sequences (1-5) showing the interactions between two deformable drops in shear flow with $\lambda = 1$, $Ca = 0.3$, $Fr = 392$, and $\eta = 0.1$

In Fig. 5 the deformation parameter of two drops are plotted as a function of dimensionless time. Points in this figure that have been shown for Ca = 0.3 correspond to the numbered sequence illustrated in Fig. 3. Drop deformation increases with η as illustrated in Fig. 5. After separation, the final equilibrium positions of drops are different at different density ratios. As the density ratio increases, the drops interact with a larger inertia force. So, the deformation of the drop increases with increasing the density ratio. But, in all cases, the deformation slightly decreases during approach, then goes through a maximum (point 2), a minimum (point4), a second maximum, and eventually reaches a steady state.

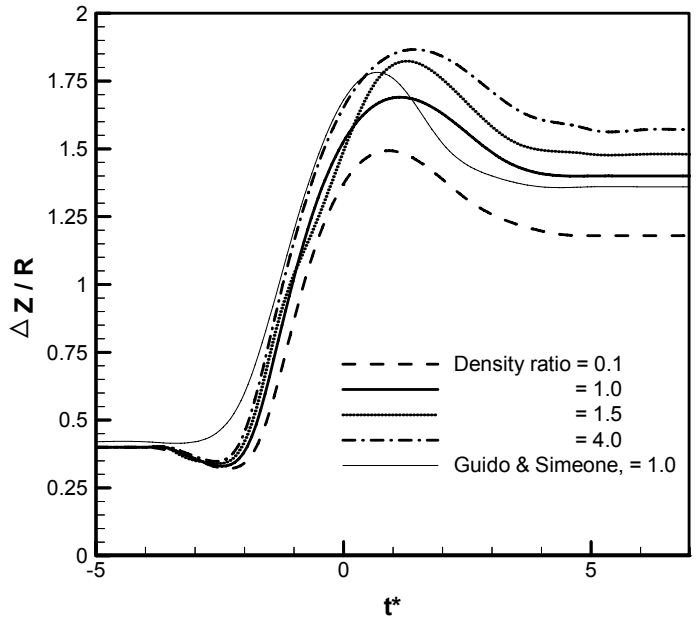

Fig. 4. Cross-flow separation (velocity gradient direction) versus dimensionless time between interacting drops at various density ratio indicated and $\lambda = 1$

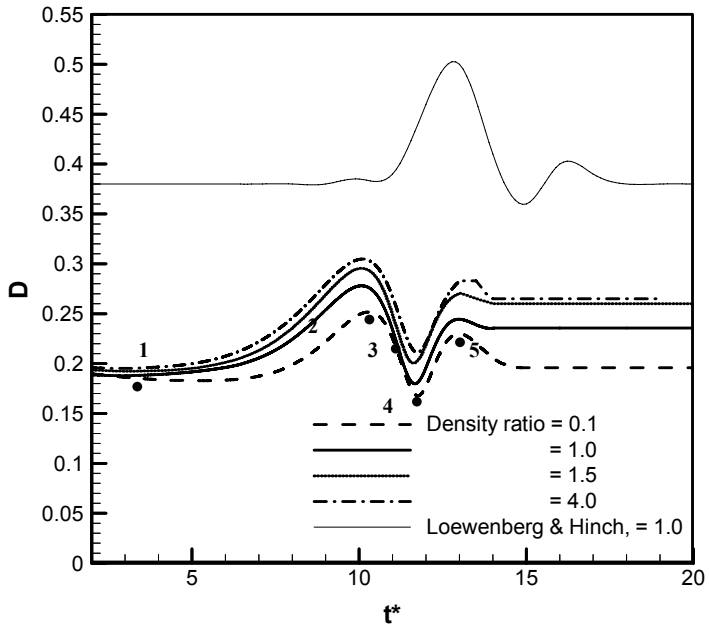

Fig. 5. Drop deformation versus dimensionless time between interacting drops with the density ratio indicated and $\lambda = 1$. Points correspond to the numbered sequences illustrated in Fig. 2

Following Allan & Mason [27], the trend shown by the deformation parameter can be explained qualitatively by considering the drops as forming a "collision doublet". The orientation angle of the doublet is defined as the angle Φ that the line joining the centres of mass of drops makes with respect to z-axis. In Fig. 6 the orientation angle Φ is plotted as a function of Δx. The limiting values of Φ are -90° for $\Delta x \rightarrow -\infty$ and $+90^\circ$ for $\Delta x \rightarrow +\infty$. The force exerted by the ambient fluid on the doublet pushes the two drops together in the compressional quadrant of shear flow ($\Phi < 0$). It increases the deformation of each drop in the compressional quadrant and this tendency is shown by the sequences in Fig. 3 and the trends in

Fig. 5. In Fig. 7 the relative velocity between the centres of mass along the flow direction, indicated as ΔV_x, and is plotted as a function of Δx. The relative velocity in the x-direction increases rapidly when the drops start interacting. This shows that drops accelerate while sliding over each other. The final steady-state value of the relative velocity along the flow direction is higher than the initial one. This is due to the increased distance between the drops along the z-axis.

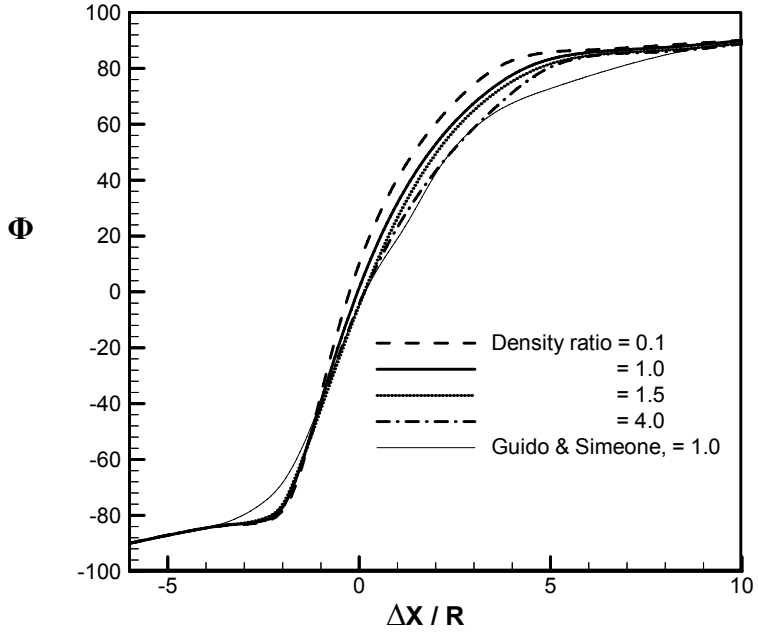

Fig. 6. The angle Φ between the line joining drop centres and x-axis versus $\Delta x / R$ with the density ratio indicated and $\lambda = 1$

If the drops were made to collide again by reversing the flow direction, Δz would increase further. In other words, the effect is irreversible.

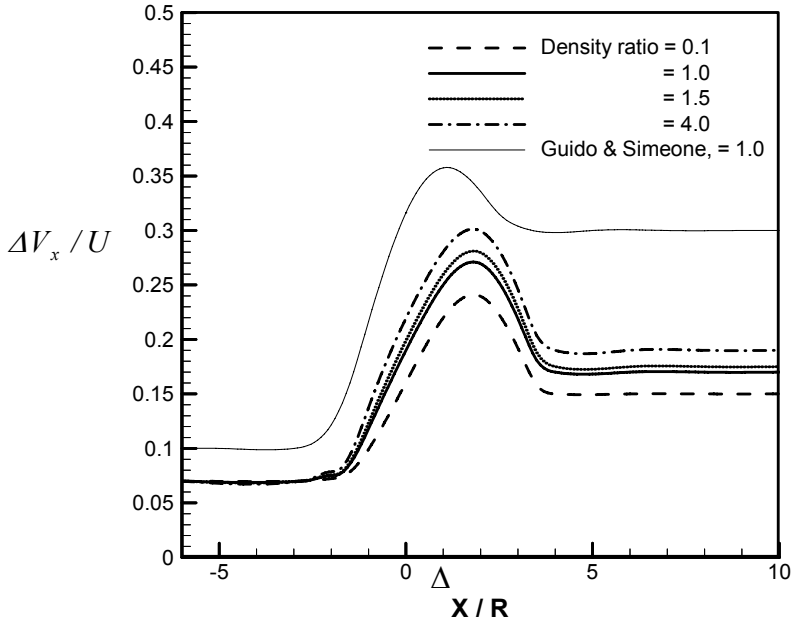

Fig. 7. The relative velocity between the drops in the x-direction versus $\Delta x / R$. (The relative velocity of Guido & Simeone's plot has been divided to 20)

When the doublet reaches the extensional quadrant, the deformation starts decreasing and reaches a minimum (point 4 in Fig. 5 and the corresponding frame in Fig. 3). The minimum value of the deformation is lower than the steady state value after collision. This is a result of two effects: (i) relaxation of drop shape at the moment that the doublet leaves the compressional quadrant and (ii) effect of the ambient fluid on the drops (Guido & Simeone [9]). The ambient fluid exerts an extensional force on the doublet.

Upon increasing Φ, the extensional effect of the ambient fluid leads to an increase of the deformation up to a maximum when drops separate. The drops then relax to the steady state without interaction. In the extensional quadrant of the shear flow, the internal circulation removes the fluid from the gap and thus tends to reduce the separation between the drops (Loewenberg & Hinch [8]). It can be seen in Fig. 6 that the orientation of the doublet is approximately the same at different density ratios.

In Fig. 8 the trajectories of drops (centre-to-centre distance scaled by the undeformed diameter) for different density ratios are plotted for an initial offset of 0.2. As the density ratio decreases, the drops rotate more slowly, and the point at which the drops separate is delayed.

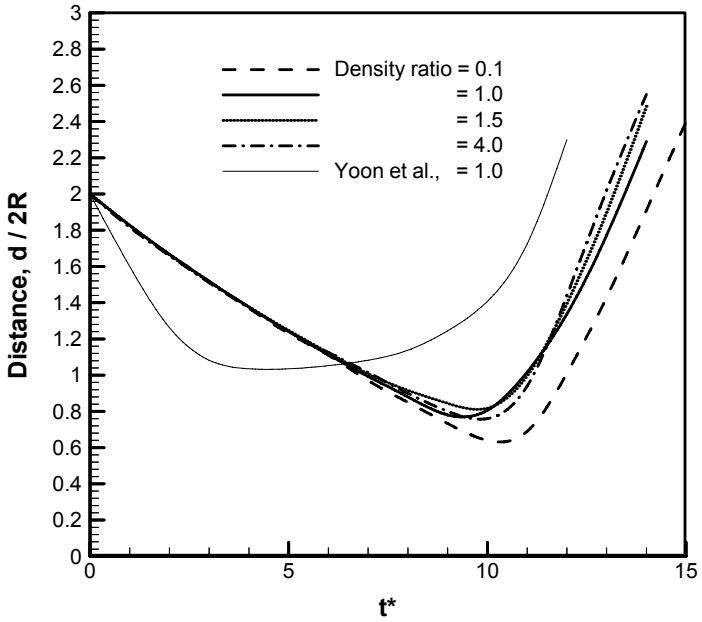

Fig. 8. Trajectories of drops for different density ratios, separation distance versus dimensionless time, with $Ca = 0.3$, $\lambda = 1$ (present work), and $\lambda = 1.2$ (experiment)

This is due to the reduction of the inertia of drops at low density ratios. The lubrication force in the thin film becomes stronger owing to the reduction of interfacial mobility caused by decrease of the density ratio. This force makes it difficult for the drops to come into contact, and the drops rotate to a larger angle before they separate significantly. The reduced inertia of drops causes a weaker interaction, which in turn makes it longer for drops to get apart from each other. In Fig. 8 the separation distance is plotted versus the orientation angle for different density ratios. We see that the approaching parts of the trajectories are different owing to different density ratios. However, after the drops come into contact, it can be seen that they follow approximately the same trajectories. This is in agreement with the experimental results of Yoon et al. [14]. They pointed out that they have no explanation for this result.

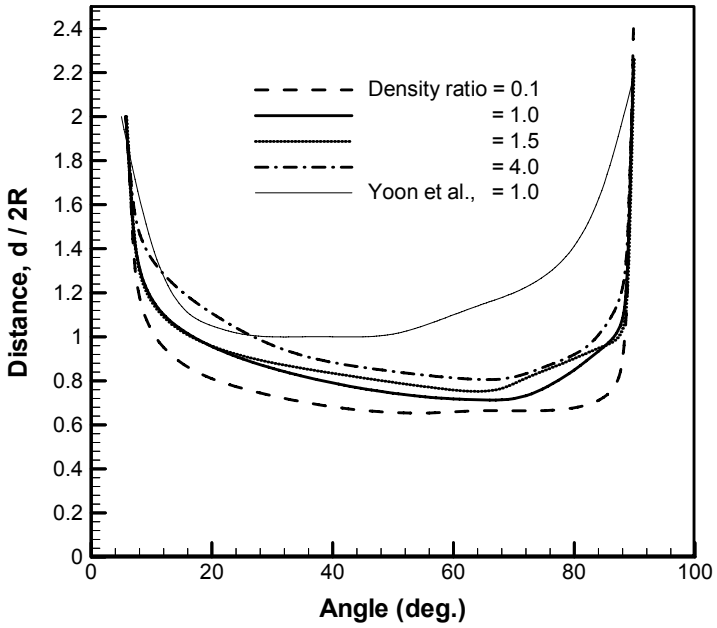

Fig. 9. Trajectories of drops for different initial offsets; separation distance versus orientation angle ($\alpha = \pi/2 - \Phi$), with $Ca = 0.3$, $\lambda = 1$ (present work), and $\lambda = 1.2$ (experiment)

4. CONCLUDING REMARKS

In this work, the interaction between two deformable drops in a shear flow has been studied over a range of density ratios considering the gravity influence. The distance Δz between the drop centres along the velocity gradient direction was plotted versus dimensionless time during three stages of the interaction: approach, collision, and separation. The results showed that the interaction between deformable drops increases the cross-flow separation of their centres. The interaction between drops is affected by the density ratio. It was found that Δz increases with increasing the density ratio. After separation, the final equilibrium positions of drops are different for different density ratios. As the density ratio increases, the relative axial velocity between the drops increases. So, the deformation of drop increases with increasing the density ratio.

For a range of density ratios, in the absence of van der Waals attraction, drop deformation prevents drop coalescence at finite Reynolds numbers; the reduced collision cross-section of the drops allows them to glide past each other. Drops accelerate while sliding over each other. This can be realized from the relative velocity between the centres of mass along the flow direction.

As the density ratio decreases, the drops rotate more slowly, and the point at which the drops separate is delayed.

REFERENCES

1. Karnis, A. & Mason, S. G. (1967). Particle motions in sheared suspensions. XXIII. Wall migration of fluid drops, *J. Colloid and Inerface. Science*, Vol. (24), pp. 164-169.
2. Feng, J., Hu, H. H. & Joseph, D. D. (1994). Direct simulation of initial value problems for the motion of solid bodies in a Newtonian fluid. Part 2. Couette and Poiseuille flows, *J. Fluid Mech*, Vol. 277, pp. 271-301.
3. Doddi, S. K. & Bagchi, P. (2008). Lateral migration of a capsule in a plane Poiseuille in a channel. *Int. J. Multiphase flow*, Vol. 34, pp. 966- 986.

4. Bayareh, M. & Mortazavi, S. (2009). Numerical simulation of the motion of a single drop in a shear flow at finite Reynolds numbers. *Iranian Journal of Science & Technology, Transaction B: Engineering*, Vol. 33, pp. 441-452.
5. Magna, M. & Stone, H. A. (1993). Buoyancy-driven interactions between two deformable viscous drops. *J. Fluid Mech.*, Vol. 256, pp. 647-683.
6. Zhou, H. & Pozrikidis, C. (1993). The flow of suspensions in channels: single files of drops. *Phys. Fluids*, Vol. A5, No. 2, pp. 311-324.
7. Li, X., Zhou, H. & Pozrikidis, C. (1995). A numerical study of the shearing motion of emulsions and foams. *J. Fluid Mech*, Vol. 286, pp. 374-404.
8. Loewenberg, M. & Hinch, E. (1996). Numerical simulation of a concentrated emulsion in shear flow. *J. Fluid Mech*., Vol. 321, pp. 395-419.
9. Guido, S. & Simeone, M. (1998). Binary collision of drops in simple shear flow by computer-assisted video optical microscopy. *J. Fluid Mech.*, Vol. 357, pp. 1-20.
10. Brenn, G., Valkovska, D. & Danov, K. D. (2002). The formation of satellite droplets by unstable binary drop collisions. *Phys. Fluids,* Vol. 13, pp. 2463–2477.
11. Motzigemba, M., Roth, N., Bothe, D., Warnecke, H. J., Prüss, J., Wielage, K. & Weigand, B. (2002). The effect of Non-Newtonian flow behavior on binary droplet collisions: VOF-Simulation and experimental analysis, *ILASS,* Zaragoza, Spain.
12. Balabel, A., Binninger, B., Herrmann, M. & Peters, N. (2002). Calculation of droplet deformation by surface tension effects using the Level Set method. *J. Combustion Science and Technology,* Vol. 174, pp. 257-278.
13. Pan, Y. & Suga, K. (2005). Numerical simulation of binary liquid droplet collision. *Phys. Fluids*, Vol. 17, pp. 1-14.
14. Yoon, Y., Borrell, M., Park, C. C. & Leal, G. (2005) Viscosity ratio effects on the coalescence of two equal-sized drops in a two-dimensional linear flow. *J. Fluid Mech.*, Vol. 525, pp. 355-379.
15. Zhao, X. (2005). Effects of inertia on the rheology of a dilute emulsion of drops in shear flow. *J. Rheology*, Vol. 49, pp. 1377-1394.
16. Sibillo, V., Pasquariello, G., Simeone, M., Cristini, V. & Guido, S. (2007). Drop deformation in micro confined shear flow. *PhysRevLett*, Vol. 97, pp. 2-4.
17. Chen, R. & Chen, C. (2006). Collision between immiscible drops with large surface tension difference: diesel oil and water. *J. Experiment in Fluids*, Vol. 41, pp. 453-461.
18. Zhao, X. (2007). Drop break up in dilute Newtonian emulsions in simple shear flow: new drop break up mechanism. *J. Rheology*, Vol. 51, pp. 367-192.
19. Lac, E. & Biesel, D. (2008). Pairwise interaction of capsules in simple shear flow: three-dimensional effects, *Physics of Fluid*. Vol. 20, pp. 040801-6.
20. Gu, X., Gupta, A. & Kumar, R. (2009). Lattice Boltzmann simulation of drop collision and surface impingement at high density ratio. *J. Thermodynamics and Heat Transfer*, Vol. 23, pp. 773-785.
21. Zhongguo, S., Guang, X. & Xi, C. (2009). Mechanism study of deformation and mass transfer for binary droplet collisions with particle method. *Phys. Fluids*, Vol. 21, pp. 032106-032106-13.
22. Nikolopoulos, N., Theodorakakos, A. & Bergeles, G. (2009). Off-centre binary collision of droplets: A numerical investigation. *International Journal of Heat and Mass Transfer,* Vol. 52, pp. 4160-4174.
23. Bayareh, M. & Mortazavi, S. (2010). Migration of a drop in simple shear flow at finite Reynolds numbers: size and viscosity ratio effects. *Proceeding of International Conference on Mechanical, Industrial, and Manufacturing Engineering (ICMIME)*, Cape Town, South Africa.
24. Bayareh, M. & Mortazavi, S. (2011). Binary collision of drops in simple shear flow at finite Reynolds numbers: geometry and viscosity ratio effects. *J. Advances in Engineering Software*, (accepted).

25. Nikolopoulos, N. & Bergeles, G. (2011). The effect of gas and liquid properties and droplet size ratio on the central collision between two unequal-size droplets in the reflexive regime, *International Journal of Heat and Mass Transfer*, Vol. 54, pp. 678-691.
26. Unverdi, S. O. & Tryggvason, G. (1992). Comutaions of multi-fluid flows. *J. Phsics*, Vol. D60, pp. 70-83.
27. Allan, R. S. & Mason, S. G. (1962). Particle motion in sheared suspensions. XIV. Coalescence of liquid drops in electric and shear fields, *J. Colloid Interface Sci.*, Vol. 17, pp. 383-408.